

FORMATION OF NARROW DUST RINGS IN CIRCUMSTELLAR DEBRIS DISKS

GURTINA BESLA^{1,2} AND YANQIN WU²

Draft version June 27, 2021

ABSTRACT

Narrow dust rings observed around some young stars (e.g., HR 4796A) need to be confined. We present a possible explanation for the formation and confinement of such rings in optically thin circumstellar disks, without invoking shepherding planets. If an enhancement of dust grains (e.g., due to a catastrophic collision) occurs somewhere in the disk, photoelectric emission from the grains can heat the gas to temperatures well above that of the dust. The gas orbits with super(sub)-Keplerian speeds inward (outward) of the associated pressure maximum. This tends to concentrate the grains into a narrow region. The rise in dust density leads to further heating and a stronger concentration of grains. A narrow dust ring forms as a result of this instability. We show that this mechanism not only operates around early-type stars that have high UV fluxes, but also around stars with spectral types as late as K. This implies that this process is generic and may have occurred during the lifetime of each circumstellar disk. We examine the stringent upper-limit on the H₂ column density in the HR 4796A disk and find it to be compatible with the presence of a significant amount of hydrogen gas in the disk. We also compute the OI and CII infrared line fluxes expected from various debris disks and show that these will be easily detectable by the upcoming Herschel mission. Herschel will be instrumental in detecting and characterizing gas in these disks.

Subject headings: hydrodynamics; instabilities; circumstellar matter; infrared: stars

1. INTRODUCTION

Observations using infrared space telescopes, such as the *Infrared Space Observatory (ISO)*, the *Infrared Astronomical Satellite (IRAS)* and recently the *Spitzer Space Telescope*, have demonstrated that many stars exhibit the “*Vega-phenomenon*,” — excess infrared radiation by orbiting dust grains heated by the central star (Zuckerman & Becklin 1993). These grains are believed to lie in optically-thin, gas-poor disks that are likely the remains of more massive protoplanetary disks (Backman & Paresce 1993; Strom & Edwards 1993). Such disks are termed ‘debris disks’ because the grains have short life-times and must be continuously regenerated by larger bodies. Famous examples of this phenomenon include Vega (Aumann et al. 1984) and β Pic (Aumann 1985, and references therein). Meyer et al. (2006) presents the most recent review of debris disk observations.

When spatially resolved, many of these disks display peculiar morphologies, including rings, holes, clumps and warps. Properties of some well-known debris disks and their host stars are summarized in Table 1. Ring-like features appear to be prevalent. In this article, we focus on the phenomenology of narrow rings, with the two most prominent examples being disks around the two A-type stars HR 4796A (Jayawardhana et al. 1998; Koerner et al. 1998; Schneider et al. 1999) and Fomalhaut (Holland et al. 2003; Kalas et al. 2005; Marsh et al. 2005). In the former case, a dust ring is seen in scattered light by HST at a distance of 70 AU away from the star with an un-resolved width < 17 AU (Schneider et al.

1999). The dust disk in Fomalhaut was resolved by HST to be distributed in a narrow belt (width \sim 25 AU) at a distance of 135 AU from the star (Kalas et al. 2005).

Narrow dust rings also appear around stars of later spectral types: the dust disks of two F-type stars, HD 139664 (F5) and HD 181327 (F5/F6) were recently resolved by HST as narrow belts, the former appears as a ring of width \sim 26 AU centered \sim 90 AU away from the star (Kalas et al. 2006), while the latter a width 36 AU at \sim 86 AU away (Schneider et al. 2006). In addition, model fitting using Spitzer spectrophotometry data indicate that dust around the solar-type star HD 105 may lie in a narrow belt (width < 4 AU) located \sim 42 AU away from the star (Meyer et al. 2004).

While HR 4796A, HD 181327 and HD 105 are relatively young (a few Myrs), the ages for Fomalhaut and HD 139664 are estimated to be \sim 10⁸ years.

Barring issues related to observational sensitivity limits, the presence of a clear outer edge for these rings is puzzling. The surface brightness of debris disks is likely dominated by grains just above the radiative blow-out size ($\beta = 1/2$, see eq. [9]). Even if these grains are produced by parent bodies on circular orbits that lie within a ring, radiation pressure launches them to eccentric orbits upon creation (with $e = \beta/(1 - \beta)$). The narrow ring geometry is destroyed within a dynamical time and one observes a greatly broadened disk with no sharp outer edge (Augereau et al. 2001; Thébault et al. 2003; Strubbe & Chiang 2006; Krivov et al. 2006; Wyatt 2006, also see §7.1). This likely explains the distribution of grain populations in AU Mic, β Pic and Vega: small grains are observed in a broad disk, whereas larger grains (detected in thermal infrared in the cases of β Pic and Vega) are observed in ring-like geometry. So why do some systems appear ring-like in scattered-light images?

The most popular explanation for ring confinement invokes one or more massive shepherding planets orbit-

¹ Harvard-Smithsonian Center for Astrophysics, 60 Garden Street, Cambridge, MA 02138, USA

² Department of Astronomy & Astrophysics, 50 St. George Street, University of Toronto, Toronto, ON M5S 3H4, Canada
Electronic address: gbesla@cfa.harvard.edu, wu@astro.utoronto.ca

TABLE 1
PROPERTIES OF SOME SPATIALLY RESOLVED DEBRIS DISKS

Star	Spectral Type	L_* (L_\odot)	Age (Myr)	χ^a	M_{dust}^b (M_\oplus)	L_{IR} (L_*)	Peak emission (AU)	Ring Width (AU)	Refs.
HR 4796A	A0	21	8 ± 2	538	≥ 0.25	5×10^{-3}	70	< 17	1,2,3,4
Vega	A0	60	350	...	0.003	2×10^{-5}	> 86	...	5,6,7,8
Fomalhaut	A3	13	100-300	...	0.017	4.6×10^{-5}	135	25	6,9,12,13
β Pic	A5	8.7	12^{+8}_{-4}	0.17	0.04	3×10^{-3}	120	90^c	10,12,15
HD 139664	F5	3.3	300^{+700}_{-200}	...	$> 8.7 \times 10^{-4}$	10^{-5}	~ 90	26	16
HD 181327	F5/F6	3.1	~ 10	...	0.05	2×10^{-3}	86	36	17,18
HD 105	G0	1.3	30 ± 10	...	~ 0.03	3.9×10^{-4}	42	4	19
HD 107146	G2	1.1	80-200	3.2×10^{-6}	0.1-0.4	1.2×10^{-3}	130	85	5,11
HD 53143	K1	0.7	1000 ± 200	...	1.2×10^{-4}	$> 1.6 \times 10^{-5}$	$\sim 55 - 110$	> 55	7,16
ϵ Eridani	K2	0.33	850	...	0.002	8×10^{-5}	65	50	12,14

REFERENCES. — (1) Jura et al. (1998); (2) Stauffer et al. (1995); (3) Greaves et al. (2000); (4) Schneider et al. (1999); (5) Williams et al. (2004); (6) Dent et al. (2000); (7) Song et al. (2000); (8) Su et al. (2005); (9) Barrado y Navascues et al. (1997); (10) Zuckerman et al. (2001); (11) Ardila et al. (2004); (12) Di Folco et al. (2004); (13) Kalas et al. (2005); (14) Greaves et al. (2005); (15) Heap et al. (2000); (16) Kalas et al. (2006); (17) Schneider et al. (2006); (18) Mannings & Barlow (1998); (19) Meyer et al. (2004).

^aThe stellar FUV (11.2 - 12.42 eV) photon flux, normalized by the average interstellar value of $1.2 \times 10^7 / \text{cm}^2 / \text{s}$ (Habing 1968), and evaluated at 70 AU from the star. The high resolution spectra are provided by Kamp & Hauschildt (Hauschildt et al. 1999), and the flux calibration is performed by Fernandez et al. (2006).

^bDust masses are estimated from sub-millimeter fluxes assuming optically thin radiation, except for HD 139664 and HD 53143 for which the dust masses were calculated from the optical depth as described in [16].

^cWe adopt here the radial profile inversion by Artymowicz (private communication) based on observations from Heap et al. (2000).

ing at distances comparable to that of the ring. As grains spiral inward due to Poynting-Robertson (P-R) drag, the gravitational tug from the planets may temporarily stall the grains at special radii (mean-motion resonances, MMR), giving rise to an apparent narrow ring (see, e.g. Ozernoy et al. 2000; Wilner et al. 2002; Quillen & Thorndike 2002; Kuchner & Holman 2003; Moran et al. 2004). The outward migration of a large planet may also trap grains in MMRs, without the need for P-R drag (see, e.g. Wyatt 2003, 2006). This process is similar to the resonance capture of Kuiper Belt objects by Neptune. Alternatively, gravitational scattering by massive planets may prevent grains from migrating across the planet's orbit, leading to a dust distribution with a sharp inner edge (Moro-Martín et al. 2005).

However, there are problems with the planet hypothesis, even if we accept the existence of giant planets at such large radii. Firstly, grain-grain collisions typically induce radial diffusion at a rate orders of magnitude above that from P-R drag, thus weakening the capture in MMRs. The sharp edges formed by planet scattering may also be smeared out by collisions. Secondly, the ability of planets to confine grains that are launched to elliptic orbits may be limited. Moran et al. (2004) noted that at eccentricities larger than that of the planet's orbit, grains spiralling inwards due to P-R drag can no longer be trapped in MMRs. Wyatt (2006) further illustrated that even grains generated by a resonant parent population will become radially spread out and azimuthally axisymmetric, so long as they are small enough to experience significant radiation pressure ($\beta \sim 1/2$). Further studies taking these effects into account are clearly warranted.

Interestingly, Wyatt (2005) argued that the process of grain-grain collisions can itself act as a potential confining mechanism for the narrow ring. For most observed debris disks, small dust grains collide destructively on

timescales much shorter than that of P-R drag. Consequently, dust generated at large distances from the central star cannot penetrate the collisional barrier to reach the inner region of the system. This produces a dust ring with a sharply defined inner-edge. If this dust ring is also optically thick in the radial direction, so that radiation pressure cannot disperse the disk (see above), it is possible for the ring to remain narrow.

Kenyon & Bromley (2002) introduced an alternative theory for ring formation. In a planetesimal disk, runaway growth occurs at successively later times further away from the star (for an overview see Nagasawa et al. 2006). Kenyon & Bromley (2002) suggested that these newly formed protoplanets gravitationally stir the left-over planetesimals, inducing violent collisions that erode the planetesimal disk. As such, at any given time the disk will appear as a broad ring with a dark inner hole (or gap). The observed rings herald the locations of recent runaway growth and the dark holes where growth has completed, or shadows where planets have yet to form (Kenyon & Bromley 2004a). The dust masses and luminosities they obtained are comparable to those in the observed debris disks (see also Kenyon & Bromley 2004b). However, if these disks are optically thin in the radial direction, the ring should not have a well-defined outer edge since the freshly produced grains will spread out in a dynamical timescale.

Krauss & Wurm (2005) recently considered a novel effect called photophoresis. They showed that in optically thin circumstellar disks with gas densities comparable to that in a minimum mass solar nebula (MMSN), grains can be pushed outward to a critical radius where the gas 'photophoretic' force equals the gas drag. The width of the resulting dust ring is, as of yet, unexplored in this model. Even so, this model faces the following two difficulties: (1) For the critical radius to be at 70 AU, the gas density needs to be twice that in the MMSN. This creates

a problem – there can be no photophoresis effect once the gas has blocked out the direct starlight. At this density, the optical depth caused by hydrogen Rayleigh scattering alone is $\tau_{\text{Ray}} = 0.4$ if integrated from 10 AU to 70 AU, and 24 if integrated from 1 AU to 70 AU (Rayleigh opacity $\kappa \sim 10^{-3} \text{ cm}^2/\text{g}$ at 4000 Å, Mayer & Duschl 2005). This model thus requires the gas disk to be truncated inward of ~ 10 AU. (2) The assumption of twice the MMSN density for the observed debris disks has been ruled out by the observed upper limits on the column densities of multiple gas species (not just hydrogen) in these disks (Greaves et al. 2000; Chen & Kamp 2004). If we assume a gas density of 2×10^{-5} MMSN instead (like that in our model), and that grains and gas are tightly coupled, the critical radius for photophoresis should be at ~ 0.2 AU (eq. [13] of Krauss & Wurm (2005)). This radius is even smaller if grains and gas are not tightly coupled. For these two reasons, we believe that photophoresis cannot explain rings in debris disks.

Along a different line, Takeuchi & Artymowicz (2001, hereafter referred to as **TA01**) suggested that rings arise naturally in disks passing through the transitional phase from gas-dominated (proto-planetary) disks to dust-dominated (debris) disks. Residual gas in these disks can be rotating with either super- or sub-Keplerian speeds depending on the local radial pressure gradient, whereas dust grains have sub-Keplerian speeds that depend on grain size. The grains therefore feel either a head-wind or a tail-wind, forcing them to migrate radially until they are in co-rotation with the gas. TA01 showed that this effect causes a local concentration of grains; in particular, when the gas pressure experiences a sharp drop-off, a narrow dust ring forms locally. In their work this pressure drop-off is provided by an artificial cut-off in gas density over a radial distance of order the disk vertical scale height.

In this study, we propose an extension to TA01’s work. We lift the undesirable assumption of an artificially-truncated gas disk and show that narrow rings form under more general initial conditions. We assume that the residual gas is smoothly distributed within the disk, but that the dust is locally enhanced. The enhancement can occur over a distance of tens of AU, e.g., as the result of a major collisional event in the underlying planetesimal disk (§2). We relax the conventional assumption of temperature equality between the gas and dust components in the disk and show that the gas heats up due to the dust enhancement. We demonstrate that this gas response leads to the confinement of the dust grains. The mechanism discussed in this paper is an instability: a slight confinement of the dust heats the gas further which leads to a stronger confinement.

Klahr & Lin (2005) (hereafter KL) have proposed a similar mechanism for the creation of narrow rings. Their analytical work assumes a simple relationship between the gas temperature and dust density, $T_{\text{gas}} \propto \rho_{\text{dust}}^\beta$ with $\beta > 0$. Our thermal analysis validates this assumption for a large range of gas/dust masses and stellar spectral types. While KL study grains of a single size and argue that narrow rings will arise from infinitesimally small perturbations of a smooth dust distribution, we study a continuous spectrum of grain sizes and a large perturbation (a dust belt). KL also speculate that the dust ring

“freezes” after it has formed, despite the disappearance of the gas as the disk evolves. This speculation needs to be assessed by taking into account radiation pressure and frequent grain collisions (see above).

In the following, we discuss the observations related to dust and gas masses in known debris disk systems (§2); these motivate our model for the transitional disk (§3). In §4, we present calculations of gas heating/cooling rates and temperatures in such a disk. Narrow dust rings are shown to arise in our fiducial model, as well as in a wide range of parameter space (§5). We discuss the best tracers for gas in these disks (§6), as well as major complications to our model (§7). We conclude in §8.

2. DUST AND GAS MASSES IN OBSERVED DEBRIS DISKS

2.1. Dust Mass

Inferred dust masses for various systems are listed in Table 1. Our fiducial value corresponds to that observed in HR 4796A. To produce $\sim 0.1M_\oplus$ of dust (size ≤ 1 mm), the parent bodies (planetesimals or proto-planets) are likely much more massive. For comparison, the current Kuiper belt has a mass of $\sim 0.1M_\oplus$, while the primordial Kuiper belt is believed to be many times more massive (perhaps up to a factor of 50).

To produce the observed infrared radiation, the dust disk must have a vertical scale height of

$$\frac{H}{r} = \frac{1}{2} \frac{L_{\text{IR}}}{L_*} \text{Max} \left(\frac{1}{\tau_r}, 1 \right), \quad (1)$$

where L_{IR}/L_* is the disk infrared to stellar optical light ratio ($\sim 5 \times 10^{-3}$ in the case of HR 4796A (Table 1) and τ_r is the radial optical depth of the dust disk. In our fiducial model, we take $H/r = 0.05$.

The vertical scale height is damped by grain-grain collisions in the collisional timescale. In our fiducial disk, dust travelling on inclined orbits will collide with grains at the mid-plane at a relative velocity of

$$\frac{v_\perp}{v_{\text{kep}}} \approx \frac{H}{r} = 0.05. \quad (2)$$

The mean free time for collisions ($T_{\text{collision}}$) can be estimated as

$$T_{\text{collision}} = \frac{1}{n_s \sigma_s v_\perp}, \quad (3)$$

where $\sigma_s = \pi s^2$ is the geometrical cross section of the grain. Only collisions between particles of similar sizes are relevant for the dynamics, thus n_s is approximately the number density of dust grains in a size bin ($s, 2s$):

$$n_s = \int_s^{2s} \frac{dn_{\text{dust}}}{ds'} ds', \quad (4)$$

where dn_{dust}/ds' is described by eq. [7]. $T_{\text{collision}}$, estimated at 70 AU, is plotted as a function of grain size in Fig. 7 (dotted line). The collision timescale for the smallest grains is ~ 20 orbits in HR 4796A.

The dust vertical velocity can also be damped by gas drag. In the weak coupling limit, this is described by the following equation,

$$\ddot{z} = \Omega_{\text{kep}}^2 z - \frac{\rho_{\text{gas}} v_{\text{th}}}{\rho_{\text{grain}} s} \dot{z}, \quad (5)$$

where z is the vertical position of the grain and v_{th} is the gas thermal speed. We take ρ_{grain} , the bulk density

of grains, to be 1.25 g/cm^3 . If this process alone is important, the vertical scale height of the dust disk decays with a timescale of $T_{\text{settle}} \sim \rho_{\text{grain}} s / \rho_{\text{gas}} v_{\text{th}}$; this is also plotted in Fig. 7.

The frequent collisions and the rapid settling by gas drag should result in a razor-thin debris disk. The observed finite thickness therefore indicates stirring (Stewart & Wetherill 1988; Kenyon et al. 1999).

However, giant planets are not necessarily required for the stirring. For instance, a Kuiper belt with individual bodies $\sim 200 \text{ km}$ in size, self-stirred to their respective surface escape velocities, and having overlapping Hill spheres, can maintain a dust scale height of $H/r \sim 0.05$. Dust is continuously wafted up by these bodies. The total number of such planetesimals required so that their Hill spheres overlap radially and vertically over a belt-width of 20 AU and scale height of $H/r = 0.05$ is $\sim 3000 \times 150$, or a total mass of $\sim 2M_{\oplus}$ (see also Kenyon & Bromley 2001; Goldreich et al. 2004). The copious amount of dust observed may also be produced by collisions between these objects.

The observed lifetime of such a massive dust disk is related to the collision time of the largest particles that are in collisional equilibrium, which is $\sim 1 \text{ Myr}$ for 1 mm particles (Fig. 7).

2.2. Gas Mass

Except for some detections of CO (Roberge et al. 2000; Dent et al. 2005), CI and CII (Roberge et al. 2000; Kamp et al. 2003; Roberge et al. 2006) and heavy metal absorption and emission lines (Olofsson et al. 2001; Brandeker et al. 2004), most gas observations of debris disks have turned up with only upper limits on the gas column density (for a review, see Jura 2004; Meyer et al. 2006). These translate to gas-to-dust ratios of less than a few (Greaves et al. 2000; Lecavelier des Etangs et al. 2001; Chen & Kamp 2004; Hollenbach et al. 2005; Roberge et al. 2005, also see §6). We set our gas-to-dust mass ratio to be in the same range.

Gas can be dissipated either via the viscous spreading associated with MHD turbulence, or by photo-evaporation (e.g. Alexander et al. 2006). In the former case, the disk dissipates gradually with a viscous timescale $\sim 10 \text{ Myr}$ (for $\alpha = 10^{-2}$ and $H/r = 0.05$ at 70 AU). HR 4796A belongs to the 8 Myr old TW Hydrae association, whose namesake TW Hydra is still actively accreting. As such, the assumption of some amount of gas in HR 4796A does not seem unreasonable.

Photo-evaporation models, on the other hand, predict that once the inner gas disk has dissipated, which occurs at $\sim 10 \text{ Myr}$ for a $2 M_{\odot}$ star with an ionizing flux of 10^{42} s^{-1} (Table 1 of Alexander et al. 2006), the outer disk disappears in a very short interval. If this is the case, our assumption of a gas disk will be difficult to justify. However, we caution that the success of the photo-evaporation models depends critically on the EUV flux, which is uncertain even for T Tauri stars. Also, while T Tauri stars (on which these models are based) are likely magnetically active and bright in EUV, this may be less true for A-type or F-type stars. If one adopts instead a flux of 10^{40} s^{-1} , the photo-evaporation timescale rises by a factor of ~ 4 and viscous evolution may dominate the evolution at the epoch of interest.

3. OUR FIDUCIAL MODEL

For our fiducial model, we consider an optically thin disk surrounding an HR 4796A-like star (A0V, $M_* = 2.5M_{\odot}$, $L_* = 21L_{\odot}$, $T_{\text{eff}} = 10,000 \text{ K}$). We assume that the disk is in the so-called ‘transitional phase’ with dust mass comparable to that of the residual gas, although the underlying planetesimal population that produces this dust can have a much greater mass. Our choices for the masses of the gas and the dust components are justified in §2.

The mass of the microscopic dust (grains with size $< 1 \text{ mm}$) is taken to be $M_{\text{dust}} = 0.1M_{\oplus} = M_{\text{gas}}$. Dust grains are initially distributed within a broad (FWHM of 20 AU) density enhancement centered at 70 AU. The mid-plane dust density goes as

$$\rho_{\text{dust}}(r) = 2.7 \times 10^{-18} \exp\left[-\frac{(r-70)^2}{2\sigma^2}\right] \text{ g/cm}^3, \quad (6)$$

where the standard deviation $\sigma = 20/2.355 \text{ AU}$. Such a distribution is motivated by the possibility of a major collisional event in the underlying planetesimal population. In this article we show that the broad dust distribution described by eq. (6) will progressively narrow into a sharp ring.

Initially, dust grains are assumed to follow a size distribution of $dn/ds \propto s^{-4}$ at every radius, where s is the grain radius. This differs from the classical $s^{-3.5}$ distribution (Dohnanyi 1969), expected from collisional fragmentation equilibrium, but is compatible with the result from zodiacal dust analysis (Fixsen & Dwek 2002) as well as the spectral fit for HR 4796A (Currie et al. 2003). With such a distribution, grains from each logarithmic size bin contribute comparably to the total mass, while the smallest grains dominate the total cross-section. Taking $s_{\text{min}} = 7.7 \mu\text{m}$ (the radiative blow-out size in the HR 4796A system, see below), and $s_{\text{max}} = 1 \text{ mm}$, with a grain bulk density of $\rho_{\text{grain}} = 1.25 \text{ g/cm}^3$, we obtain the following number distribution,

$$\frac{dn_{\text{dust}}}{ds}(r, s) = 1.0 \times 10^{-19} \exp\left[-\frac{(r-70)^2}{2\sigma^2}\right] s^{-4}. \quad (7)$$

The radial optical depth for this dust disk is ~ 0.14 . Our calculations take into account the associated attenuation of starlight.

The dust temperature can be approximated by the temperature of the smallest grain at a given radius (also see eq. 28 of Kamp & Bertoldi 2000),

$$T_{\text{dust}} = 282.5 \text{ K} \left(\frac{L_*}{L_{\odot}}\right)^{\frac{1}{5}} \left(\frac{r}{\text{AU}}\right)^{-\frac{2}{5}} \left(\frac{s_{\text{min}}}{\mu\text{m}}\right)^{-\frac{1}{5}}. \quad (8)$$

These grains are slightly hotter than the corresponding blackbody temperature because they are perfect absorbers of stellar photons but inefficient emitters of their own thermal radiation.

The ratio between the radiation pressure and the gravity acting on the grain reads as,

$$\beta = \frac{3L_* Q_{\text{PR}}}{16\pi GM_* c s \rho_{\text{grain}}} = 0.46 \left(\frac{\mu\text{m}}{s}\right) \frac{L_*}{L_{\odot}} \frac{M_{\odot}}{M_*}, \quad (9)$$

where c is the speed of light and $Q_{\text{PR}} \sim 1$ is the radiation pressure efficiency averaged over the stellar spectrum. The size of the smallest grain is determined by setting

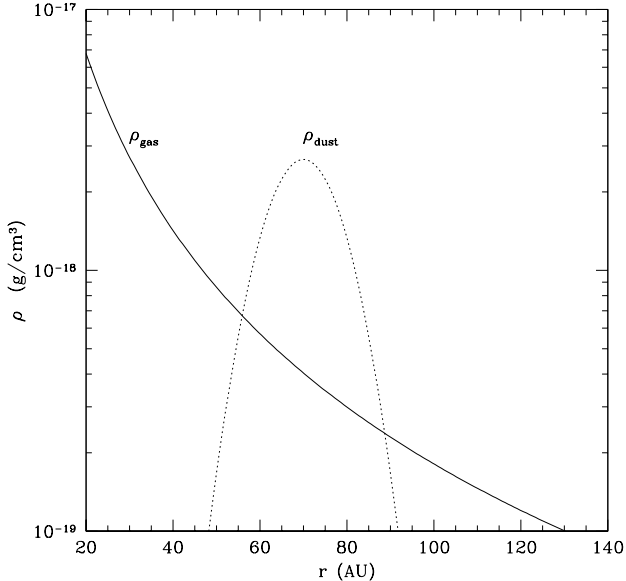


FIG. 1.— The mid-plane gas and dust densities in our transitional phase disk. While the gas density (solid line) falls off as a smooth power-law, the dust density (dotted line) is a Gaussian centered at 70 AU, with a FWHM of 20 AU. The gas and dust masses are $M_{\text{gas}} = M_{\text{dust}} = 0.1M_{\oplus}$ and both components have the same vertical scale-height of $H = 0.05r$. We stress that although we use these densities for our fiducial parameters, the proposed mechanism works over a large range of gas and dust masses (§5).

$\beta = 0.5$.³ For an A0V star such as HR 4796A, this yields $s_{\text{min}} \approx 7.7 \mu\text{m}$. We assume that grains move only on circular orbits, which limits our study to axi-symmetric features; see §7.1 for a discussion on eccentricity damping of the grains. Under this assumption, the dust orbital velocity (v_{θ}) is reduced from the local Keplerian value ($v_{\text{kep}} = \sqrt{GM_*/r}$) to

$$v_{\theta} = v_{\text{kep}}(1 - \beta)^{1/2}. \quad (10)$$

Our gas disk has a total mass of $M_{\text{gas}} = 0.1M_{\oplus}$ and satisfies a mid-plane radial density profile

$$\rho_{\text{gas}}(r) = 4.0 \times 10^{-19} \left(\frac{r}{70\text{AU}} \right)^{-2.25} \text{ g/cm}^3, \quad (11)$$

where r is the radial distance from the star (measured in AU from now on). As will become clear, the total mass and density profile for the gas disk matter little for our theory. What is relevant is the gas density at 70 AU and the fact that it is smoothly distributed over a broad region. We adopt a scale height of $H/r = 0.05$ for the gas disk, and relate surface density to mid-plane density simply as $\Sigma = 2\rho H$. From now on we ignore the vertical structure of the disk and consider only physical quantities measured at the disk mid-plane. We also impose an inner and outer cut-off to the disk at 10 and 150 AU, respectively. These cut-offs are far from the region of interest and do not affect the dynamics. The gas density is plotted as a function of radius in Figure 1.

³ Here, we define the blow-out size (s_{min}) to be the size of the largest grain that escapes to infinity when released on a circular orbit.

The gas temperature is determined by various heating and cooling processes (§4). The stellar FUV flux (11.2-12.42 eV) is relevant for many gas heating processes. Using high resolution stellar spectra provided by Kamp & Hauschildt, Fernandez et al. (2006) obtain a value of $\chi = 538$ for HR 4796A, where χ is the stellar FUV flux measured at 70 AU, normalized by the Habing ISM field ($F_{\text{H}} = 1.2 \times 10^7 / \text{cm}^2 / \text{s}$). This is somewhat larger than the $\chi = 460$ (11.2-13.6 eV) value computed by Chen & Kamp (2004) from FUSE spectra. We adopt the latter value here.

The most important gas heating rate in our disk model is photoelectric heating by dust grains. The relevant photon energies for this process range from $W + e\Phi$ to 13.6eV, where W is the grain work function ($W \sim 8\text{eV}$ for silicate grains, and $\sim 4.4\text{eV}$ for carbonaceous grains, Weingartner & Draine 2001) and Φ is the electrostatic potential of the grain. The value of Φ depends (weakly) on stellar spectrum, local electron density and gas temperature. It is important not to limit the photon energy range to the FUV range (more below).

Gas orbiting around a star is subject to the forces of gravity and gas pressure. We again assume that gas moves only on circular orbits. The gas circular velocity (v_{gas}) is

$$v_{\text{gas}} = v_{\text{kep}}(1 - \eta)^{1/2}, \quad (12)$$

where

$$\eta = -\frac{r}{v_{\text{kep}}^2 \rho_{\text{gas}}} \frac{dP}{dr}. \quad (13)$$

Here, $P = \rho_{\text{gas}} k T_{\text{gas}} / \mu_g m_H$ is the gas pressure, and we take $\mu_g = 2.34$ (for a mixture of molecular hydrogen and helium).

A grain that is orbiting faster than the local gas ($v_{\theta} > v_{\text{gas}}$) experiences a head-wind, loses angular momentum and migrates inward, and *vice versa*. Grains tend to migrate to stable orbits where they are in co-rotation with the gas, $\eta(r) = \beta(s)$. This leads to a size segregation, $s = s(r)$. This is the dynamical basis for our theory.

Let the original surface brightness of a face-on disk be approximated by the following expression,

$$I(r) = \frac{L_*}{4\pi r^2} 2H \int_{s_{\text{min}}}^{1\text{mm}} \pi s^2 \frac{dn_{\text{dust}}}{ds} ds, \quad (14)$$

where L_* is the stellar luminosity and H the dust scale-height. We set $H/r = 0.05$ as for the gas disk. We have also taken the grain albedo to be unity and assumed that the disk is face-on. After radial migration, grains of size between s and $s+ds$ (where $s > 7.7 \mu\text{m}$) are concentrated into an annulus between r and $r+dr$. Ignoring collisional evolution during this process, the dust mass within each ds bin is conserved. This yields a new surface brightness profile:

$$I(r) = \frac{L_*}{4\pi r^2} \pi s^2 \frac{ds}{dr} \frac{N_s}{2\pi r}, \quad (15)$$

where $N_s ds$ is the total number of grains between s and $s + ds$ integrated over the whole disk,

$$N_s = \int \frac{dn_{\text{dust}}}{ds} 2\pi r' 2H dr'. \quad (16)$$

4. GAS TEMPERATURE

Here, we compute gas heating and cooling rates to determine the gas temperature profile. Much of this analysis is based on the work of Kamp & van Zadelhoff (2001, hereafter referred as **KvZ01**) although we do find some disagreements with their analysis. Except where noted, we adopt their expressions to calculate various rates.

As grains migrate to their stable radii, the gas temperature profile evolves, modifying the grains' destination. We do not attempt to trace this behavior by solving the time-dependent equations self-consistently. Instead, we approach the problem by studying systems with dust distributions of differing initial FWHM.

Results at the disk mid-plane are plotted as functions of radius in Fig. 2. The equilibrium gas temperature is obtained by demanding that the local heating and cooling rates balance. The resulting temperature profile dictates the grain migration (§5). Unlike KvZ01, we ignore heating from grain drifting (see below).

4.1. Heating

KvZ01 conclude that the relevant gas heating processes in an optically thin circumstellar disk around A-stars include collisional de-excitation of H_2 , photo-dissociation of H_2 , H_2 formation on grains, gas-grain collisions (when the grain is hotter than the gas), photoelectric emission from dust grains and cosmic ray heating.

While KvZ01 used a fitting formula (their eq. [11]) to estimate the photoelectric heating rate, we opt for a full calculation that follows the procedure in Draine (1978) and Weingartner & Draine (2001). Our results differ markedly from those obtained by KvZ01 (see below).

The photoelectric charging current per dust grain (of radius s) is

$$J_{\text{pe}} = \pi s^2 e \int_{(e\phi+W)/h}^{\nu_{\text{max}}} d\nu Q_{\text{abs}} Y(h\nu) \frac{F_\nu}{h\nu} \times \left[\int_{e\phi}^{h\nu-W} f(E, h\nu) dE \right], \quad (17)$$

where W is the work function and ϕ is the charging potential of the grain. We assume that the dust disk is composed of 100% carbonaceous grains ($W = 4.4$ eV). Including silicon grains ($W = 8$ eV) does not significantly change the photoelectric heating rate (see §5). We adopt an overall absorption coefficient of $Q_{\text{abs}} = 1$, a photoelectric yield $Y(h\nu) \approx (1 - W/h\nu)/2$ and describe the electron energy distribution as $f(E, h\nu) = 6E/(h\nu - W)^2 (1 - E/(h\nu - W))$ (Weingartner & Draine 2001). F_ν is the stellar energy flux measured at the grain's location, where the central star is assumed to be a blackbody of the appropriate temperature (10,000 K for the fiducial model). F_ν is also attenuated by the radial dust optical depth. ν_{max} is the upper frequency cut-off of the stellar spectrum and is set at an energy of 13.6 eV.

The charging potential is obtained by equating eq. [17] to the thermal electron collection current,

$$J_e = 4\pi s^2 e s_e n_e \sqrt{\frac{k_B T_{\text{gas}}}{2\pi m_e}} \left(1 + \frac{e\phi}{k_B T_{\text{gas}}} \right). \quad (18)$$

This is valid when the grains are positively charged ($\phi > 0$), which is the case for the gas density of interest. We take an electron sticking coefficient of $s_e = 1$.

The factor of $4\pi s^2$ arises here because the grain receives electrons isotropically, while it intercepts photons only on the side facing the star (hence the factor πs^2 in eq. [17]). The relevant photons for the photoelectric effect lie in the UV/FUV range, where stellar flux decreases (\sim) exponentially with wavelength. The net result is that the charging potential depends weakly (almost logarithmically) on the electron density (n_e), gas temperature (T_{gas}) and radial distance from the star (see Fernandez et al. 2006). Moreover, each grain is charged to a potential that is independent of its size. An easy result to remember is that $e\phi \sim$ a few $k_B T_\star \gg k_B T_{\text{gas}}$ over the disk.

Short of calculating the full ionization balance in the transitional disk, we assume that hydrogen and carbon alone contribute to the electron density (n_e). Contributions from molecules and grains are irrelevant in our low surface density disk (at 70 AU, surface density $\sim 10^{-5}$ g/cm²). The ionization fraction of hydrogen is determined by balancing the primary cosmic ray ionization rate, $\sim 10^{-17}$ s⁻¹ (Spitzer & Tomasko 1968), with the rate of recombination (with recombination coefficient $8 \times 10^{-11}/\sqrt{T_{\text{gas}}}$ cm³/s, Osterbrock & Ferland 2006). Carbon, with a first ionization potential of 11.2 eV, is assumed to be 50% ionized.⁴ Thus,

$$n_e = n_e[\text{H}] + n_e[\text{C}] = \sqrt{\frac{10^{-17}}{8 \times 10^{-11}} T_{\text{gas}}^{1/2} n[\text{H}_{\text{tot}}] + 0.5n[\text{C}]}, \quad (19)$$

where $n[\text{H}_{\text{tot}}]$ and $n[\text{C}]$ are the number densities of hydrogen and carbon nuclei; in our model, hydrogen and carbon contribute comparably to the electron density.

The associated photoelectric heating rate is

$$\Gamma_{\text{pe}} = \pi s^2 \int_{(e\phi+W)/h}^{\nu_{\text{max}}} d\nu Q_{\text{abs}} Y(h\nu) \frac{F_\nu}{h\nu} \times \left[\int_{e\phi}^{h\nu-W} (E - e\phi) f(E, h\nu) dE \right], \quad (20)$$

where each ejected electron leaves the grain with a kinetic energy of $E - e\phi$.

A simple way to estimate Γ_{pe} , which also clarifies the parameter dependences, is to set $\Gamma_{\text{pe}} \sim J_e (1\text{eV}/e)$. In other words, each photo-electron carries ~ 1 eV of energy out of the grain towards heating the gas. All other factors being equal, two stars that have photon fluxes differing by orders of magnitude can have comparable photoelectric heating rates (§5).

When grains span multiple sizes,

$$\Gamma_{\text{pe}} = \int_{s_{\text{min}}}^{s_{\text{max}}} ds \frac{dn}{ds} \pi s^2 \int_{(e\phi+W)/h}^{\nu_{\text{max}}} d\nu Q_{\text{abs}} Y(h\nu) \frac{F_\nu}{h\nu} \times \left[\int_{e\phi}^{h\nu-W} (E - e\phi) f(E, h\nu) dE \right]. \quad (21)$$

Comparing the above heating rate against that of KvZ01, we find that, for the same parameters, our rates are typically a factor of 20 – 1000 times greater. If we

⁴ This is found to be true for the β -Pic disk (Fernandez et al. 2006). This fraction rises somewhat around hotter stars (like HR 4796A), and when the gas density (and hence the recombination rate) is decreased. We have not attempted to model this in detail.

adopt instead a cooler stellar spectrum, e.g. that of β Pic, the difference increases to a factor of $10^3 - 10^5$. This difference arises because KvZ01 used a fitting formula that only includes the FUV flux ($h\nu \geq 11\text{eV}$). This is suitable for the hotter interstellar radiation field), but in circumstellar environments, the star emits copious amounts of soft UV photons (between 4.4eV and 10eV) which are much more relevant for grain charging and photoelectric heating. Similar to our study, Gorti & Hollenbach (2004, appendix C4) have also considered stellar flux between 6 eV and 13.6 eV.

KvZ01 also report that the heating rate due to grain drift relative to the gas greatly exceeds the photoelectric heating rate. We find it to be unimportant in our calculations. The enhanced photoelectric heating aside, the drift velocity is also lower in our calculations because the dust and gas are weakly coupled. A similar conclusion was also drawn by Gorti & Hollenbach (2004).

Another important heating rate comes from gas-grain collisions. From eq. [19] of KvZ01,

$$\Gamma_{gg} = 4.0 \times 10^{-12} n[\text{H}_{\text{tot}}] \alpha_T \sqrt{T_{\text{gas}}} \times (T_{\text{dust}} - T_{\text{gas}}) \int_{s_{\text{min}}}^{s_{\text{max}}} \pi s^2 \frac{dn_{\text{dust}}}{ds} ds, \quad (22)$$

where $\alpha_T \approx 0.3$ is the thermal accommodation coefficient. Gas-grain collisions can contribute to either heating or cooling, depending on the relative values of T_{gas} and T_{dust} .

To calculate H_2 -related rates (H_2 photo-dissociation, H_2 formation and collisional de-excitation), we need to know the ratio of atomic to molecular hydrogen in the disk. This is determined by assuming that the H_2 photo-dissociation and formation rates are in equilibrium. This is a valid approach for a star like HR 4796A, where the photo-dissociation timescale ($\sim 10^3$ yrs at 70 AU) is much shorter than the system lifetime. The relevant stellar photons for H_2 photo-dissociation are in the FUV range ($> 11\text{eV}$) and their flux is characterized by the value of χ in Table 1. We include self-shielding of the stellar FUV flux by H_2 in the disk, as well as the shielding by dust. The former accounts for the fall-off in the H_2 photo-dissociation rate after the initial rise, seen in Fig. 2. In chemical equilibrium, H_2 formation contributes ~ 4 times more heating than H_2 destruction.

The conclusion that photoelectric heating is the dominant heating mechanism in optically thin disks has also been reported by Jonkheid et al. (2004) and Kamp & Dullemond (2004a). Furthermore, in contrast to the case of proto-planetary disks, the low gas density here implies that collisions between gas and grains cannot cool the gas efficiently. Instead, the gas is heated to temperatures well above the local dust temperature.

4.2. Cooling

The low gas density environment considered here is analogous to the surfaces of protoplanetary disks. Cooling is contributed by atomic fine structure lines from OI, CII, FeII and SiII, and possibly molecular transitions from H_2 , CO, H_2O and OH, as well as gas-grain collisions (Kamp & van Zadelhoff 2001; Gorti & Hollenbach 2004; Kamp & Dullemond 2004a; Jonkheid et al. 2004; Kamp & Dullemond 2004b). Among these, we include only the two most important processes: CII

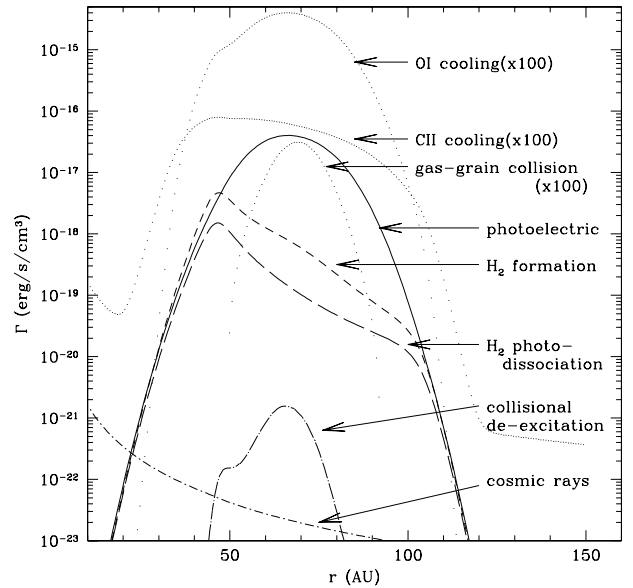


FIG. 2.— Gas heating and cooling rates are plotted as functions of radius for the transitional disk around an HR 4796A-like star (A0). The gas is assumed to be at local thermal equilibrium. All cooling rates have been increased by a factor of 100 to distinguish them from the heating rates. At the peak of the dust enhancement (70 AU), photoelectric heating and OI cooling are the dominant heating and cooling processes, respectively. Gas-grain collisions act as a cooling mechanism within the vicinity of the dust enhancement and as a heating rate outside (not plotted). Cosmic-rays dominate the heating outside the dust belt. H_2 -related rates are calculated assuming local chemical equilibrium between atomic and molecular hydrogen; in the absence of dust, starlight quickly photo-dissociates all molecular hydrogen. The asymmetric shapes of the H_2 -related rates around 70 AU are caused by H_2 self-shielding of the stellar FUV flux.

and OI. FeII ($26\mu\text{m}$) & SiII ($35\mu\text{m}$) can contribute a comparable amount to the cooling only when the gas temperature exceeds $\sim 400\text{K}$. Given the harsh UV environment, CO, H_2O and OH are rapidly photo-dissociated (Kamp & Bertoldi 2000; Lecavelier des Etangs et al. 2001) and are negligible for cooling. In comparison, H_2 is abundant since it is continuously re-formed on grain surfaces. However, the lack of dipole moment and the widely spaced energy levels preclude it from being an important coolant (Hollenbach & McKee 1979; Gorti & Hollenbach 2004).

With a transition wavelength of $158\mu\text{m}$, fine structure cooling by CII is relevant only for gas cooler than $\sim 100\text{K}$. At hotter temperatures, the fraction of CII occupying the higher level reaches unity and the CII cooling rate saturates. OI fine-structure cooling (dominant line at $63\mu\text{m}$) kicks in at these temperatures. This rate saturates in turn at $\sim 500\text{K}$.

We assume standard ISM abundances for carbon and oxygen, $n[\text{C}] = 1.4 \times 10^{-4} n[\text{H}_{\text{tot}}]$ and $n[\text{O}] = 3.2 \times 10^{-4} n[\text{H}_{\text{tot}}]$, respectively. Also, following the results in Fernandez et al. (2006), we take carbon (ionization potential of 11.2eV) to be 50% ionized and oxygen (13.6eV) to be 100% neutral. We calculate occupation levels for CII and OI assuming local thermal equilibrium (LTE);

the Einstein coefficients and statistical weights are listed in Table 1 of KvZ01. When the gas density is below a critical value, LTE is inaccurate as the higher levels may not be sufficiently collisionally populated (for more details, see KvZ01). In our model, the gas density at 70 AU ($n[\text{H}_{\text{tot}}] \approx 10^5 \text{ cm}^{-3}$) lies just below the critical density for LTE. So our faulty LTE assumption overestimates the true cooling rates and underestimates the resulting gas temperature – a more detailed treatment will further strengthen the instability described here.

We have also verified that these infrared lines are optically thin in the vertical direction.⁵

When the gas temperature exceeds the dust temperature, gas-grain collisions act as a cooling mechanism for the gas. In our fiducial model, this cooling rate is subordinate to line cooling. However, in denser disks, this cooling process likely dominates.

5. THE INSTABILITY

The gas temperature profile obtained by balancing realistic heating and cooling rates is shown in Fig. 3. Following the method outlined in §3, we compute the gas and dust orbital velocities, determine the locations of the stable orbits for different grain sizes, and calculate the new surface brightness profile (Fig. 3). The latter is more narrowly peaked around 70 AU, with a FWHM of 10 AU, compared to the 20 AU FWHM of the initial distribution. More significantly, the new dust belt has both sharp inner and outer edges.

We also perform the same analysis with a narrower initial dust distribution (FWHM = 10 AU); results are shown in Fig. 4. The higher initial dust density in the enhancement raises the photoelectric heating rate and consequently the gas temperature. The final surface brightness is strongly peaked around 70 AU with a FWHM of 5 AU. Although we have not self-consistently traced the gas temperature evolution as the dust migrates, the result of this exercise suggests that the segregation and migration of grains acts as a positive feedback, leading to further evolution (also see Klahr & Lin 2005). As such, the mechanism we discuss here is an instability.

The profile of specific angular momentum (dashed line in the middle panel of Fig. 3) decreases outwardly near 70 AU. In this region, the gas disk will be Rayleigh unstable and mix. As a result, the pressure profile will likely be somewhat reduced and the minimum width of the dust ring may be limited to ~ 10 AU.

Two key parameters in this analysis are the gas and dust densities (n_g , n_d). The photoelectric heating rate scales roughly as $n_g n_d$,⁶ while the gas line cooling rates scale as n_g . So the gas temperature profile is relatively independent of gas density, but rises with dust density. In addition, the minimum size of confinable grains ($\beta < \eta_{\text{max}}$) decreases with higher dust density (also see above).

We find that ring formation can occur over a very large range of dust mass: if we set an artificial limit of $T_{\text{max}} =$

⁵ For disks with much higher masses, these lines can become optically thick. This is accounted for by reducing the cooling flux by a factor τ .

⁶ The actual rate rises somewhat slower than this because the electron density increases slower than the gas density (eq. [19]). Also, when the gas density reaches MMSN values, grains become negatively charged. This leads to a Coulomb barrier that significantly reduces the electron collection current.

$T_{\text{dust}} \sim 60$ K for ring formation, the minimum dust mass is $\sim 0.005 M_{\oplus}$. The upper end for the dust mass is limited by dust opacity: the dust disk becomes optically thick for $M_{\text{dust}} \geq 0.7 M_{\oplus}$. The range of gas mass over which this can occur is equally wide: the minimum gas mass is set by the constraint that gas is dynamically important, i.e., $M_{\text{gas}} \geq M_{\text{dust}}$, and the maximum gas mass approaches that of the MMSN value. At this value a few effects set in to diminish the instability including: the optical depth due to gas opacity, the negative charging potential for the grains and the increasingly important gas-grain collisional cooling.

Ring formation is effective for an initial dust belt spread out as wide as 40 AU and is not significantly affected when a background population of dust (with 1% of the local gas mass) is superimposed.

Other parameters, such as grain composition and spectral type, do not have a significant impact on our model. Since the work function for silicate grains is 8eV – much greater than the 4.4eV for graphite – photons capable of striking electrons out of silicate grains must be more energetic and therefore less numerous. As a result, the charging potential (Φ) for silicate grains is typically lower by a factor of ~ 2 , which leads to a factor of ~ 2 reduction in the photoelectric heating rate (§4.1). Similarly, although stars with later spectral types output drastically decreasing amounts of UV/FUV flux, the grain charging potential, the electron density and the kinetic energy carried away by each electron only vary mildly between them. Indeed we find that bright, narrow rings may form around stars with a spectral type as late as K2.

6. HOW TO FIND THE GAS?

The gas mass is a critical unknown in our model. If gas is indeed present, what is the best way to look for it in debris disks?

In Table 2 we calculate some gas observables. We assume the same fiducial parameters (e.g., gas and dust masses of $0.1 M_{\oplus}$ as in §3), except for the characteristics of the central star (distance, luminosity and temperature). We argue below that in some cases the H_2 column densities may not be a good indicator of gas, while OI and CII fluxes (observable with Herschel) are excellent tracers.

• H_2 Column Densities

H_2 column densities have been traditionally used to place stringent upper limits on the gas mass. For instance, the non-detection of absorption in HR 4796A establishes the following $3 - \sigma$ upper-limits on the column densities of hydrogen: for H_2 occupying the two lowest rotational levels, $N[\text{H}_{2,J=0}] \leq 10^{15} \text{ cm}^{-2}$ and $N[\text{H}_{2,J=1}] \leq 3.7 \times 10^{15} \text{ cm}^{-2}$ (Chen & Kamp 2004).

The HR 4796A disk plane is inclined by $\sim 17^\circ$ from our line-of-sight (Schneider et al. 1999), i.e., for $H/r = 0.05$, the line-of-sight passes ~ 5 vertical scale heights above the mid-plane. If the gas at 70 AU is isothermal with $T \sim 200$ K (Fig. 3) and is in vertical hydrostatic equilibrium, then the gas scale height is $H_{\text{gas}} \sim 23 \text{ AU} \gg H_{\text{dust}} \sim 3.5 \text{ AU}$. If the gas at high altitudes has the same molecular to atomic ratio as that in the mid-plane, the

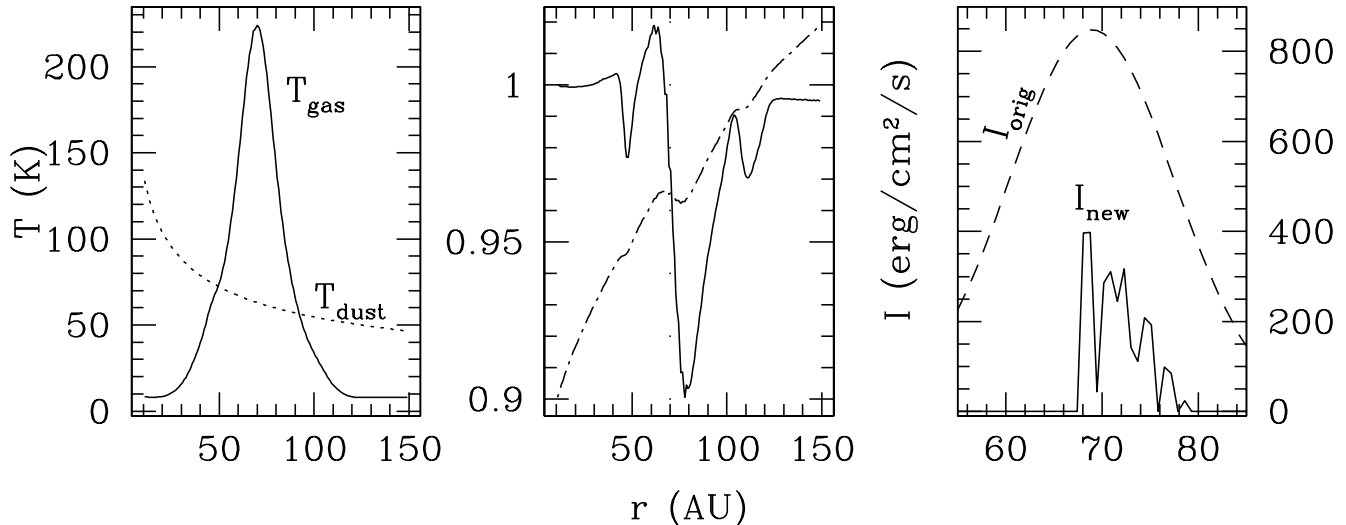


FIG. 3.— Thermal response of the gas disk as in Fig. 2. The left panel shows gas and dust temperatures as functions of radius (in AU), center panel shows the corresponding gas velocities (eq. [28]), normalized by the local Keplerian velocity. The dotted line marks the centroid (70 AU) of the dust belt; while the dashed curve indicates the profile of specific angular momentum (in arbitrary unit). Gas with outwardly decreasing angular momentum suffers from Rayleigh instability; we expect gas in these regions to mix rapidly and somewhat reduce the temperature gradient. The right panel depicts the surface brightness of a face-on disk: the dashed curve is the original surface brightness profile, while the solid one is the profile after the grains have migrated to their stable orbits. The surface brightness profile resulting from dust migration (I_{new} , right panel) is sharply concentrated around 70 AU with a FWHM of ~ 10 AU. The fluctuations seen are numerical artifacts.

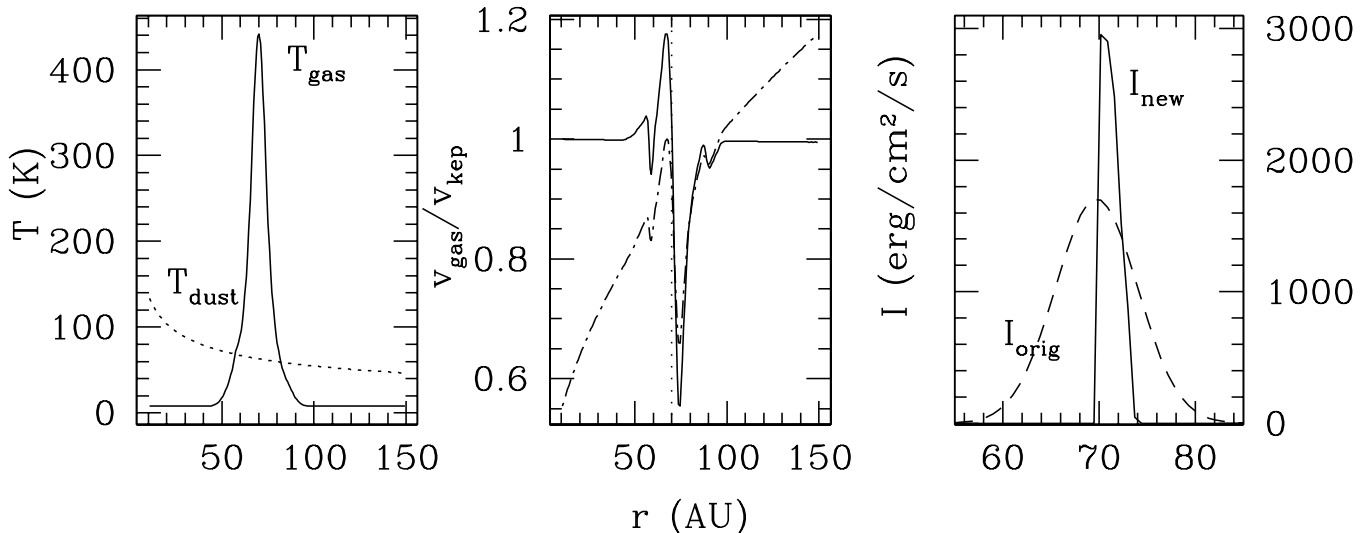


FIG. 4.— Same as Fig. 3 but the dust is initially distributed within a narrower region (FWHM = 10 AU). Both the peak temperature and the maximum η reach higher values than those in Fig. 3. The final surface brightness profile is narrowly confined between 70 and 75 AU – the ring progressively narrows.

line-of-sight column density of H_2 will be $N[\text{H}_2] = 1.2 \times 10^{19} \text{ cm}^{-2}$ in our model. This is much greater than the observed limit. Does this rule out the presence of a significant amount of gas in the HR 4796A disk?

The gas thermal timescale at 70 AU ($=nk_B T/\Gamma \sim 20$ yrs for $T = 200$ K, where Γ is the heating rate) is short compared to the dynamical time (~ 400 yrs at 70 AU), so gas rising to high altitudes will fall beyond the influence of the dust and cool rapidly. The vertical isothermal assumption is therefore invalid

and we do not expect much vertical expansion of the gas disk. Instead, $H_{\text{gas}} \sim H_{\text{dust}} \sim 3.5$ AU. This reduces the line-of-sight column density to $N[\text{H}_2] \sim 7 \times 10^{15} \text{ cm}^{-2}$. Furthermore, H_2 molecules located well above the disk mid-plane are destroyed rapidly and the ratio of molecular to atomic species is reduced compared to that at the mid-plane. We therefore conclude that the observed upper limit on $N[\text{H}_2]$ cannot yet exclude the presence of a significant amount of gas in the disk. The upper limits on other gases (Chen & Kamp 2004) are less constraining than that of H_2 and are compatible with

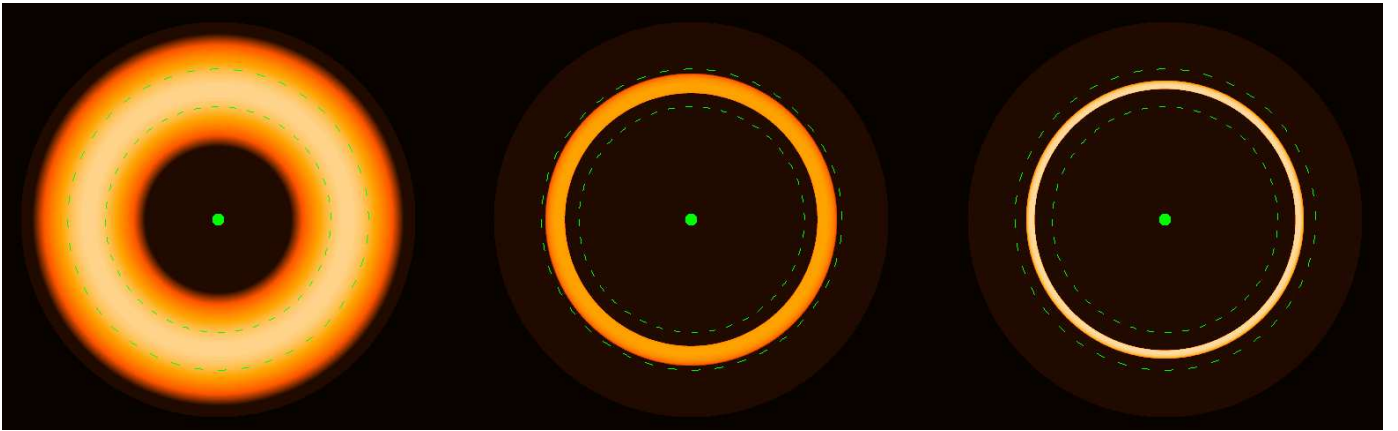


FIG. 5.— A graphical demonstration of the evolution of the dust ring, seen in scattered light. The surface brightness profiles are taken from Figs. 3-4 with the color white indicating brighter regions. The initial dust enhancement (left) has a FWHM of 20 AU. The gas within the enhancement heats up and concentrates grains into a distribution with a smaller FWHM (10 AU, center image) and sharp inner and outer edges. Subsequent evolution of this new distribution produces a bright ring with a FWHM of 5 AU. We have assumed that small grains are regenerated from larger grains after being initially lost from the system.

TABLE 2
LTE PREDICTIONS FOR VARIOUS DEBRIS DISKS

Star/Spec. Type	Distance (pc)	Column Densities ^a (cm^{-2})		Line Fluxes at Earth ^b ($\text{erg}/\text{cm}^2/\text{s}$)			
		$\text{N}[\text{H}_2]$	$\text{N}[\text{H}]$	OI($44.1 \mu\text{m}$)	OI($63.2 \mu\text{m}$)	OI($145.5 \mu\text{m}$)	CII($157.7 \mu\text{m}$)
HR 4796A(A0)	67	1.0×10^{20}	1.9×10^{21}	7.4×10^{-20}	1.9×10^{-14}	3.0×10^{-16}	5.3×10^{-16}
β Pic(A5)	19	2.3×10^{20}	1.7×10^{21}	7.7×10^{-20}	2.1×10^{-13}	3.1×10^{-15}	6.0×10^{-15}
HD 105(G0)	40	9.3×10^{20}	2.7×10^{20}	8.9×10^{-21}	2.9×10^{-14}	3.5×10^{-16}	1.2×10^{-15}
HD 107146(G2)	28.5	6.2×10^{20}	9.0×10^{20}	1.7×10^{-20}	5.6×10^{-14}	6.8×10^{-16}	2.3×10^{-15}

^aColumn densities for molecular and atomic hydrogen assuming that the disk is edge-on and that molecular and atomic hydrogen are in chemical equilibrium. The latter assumption may not be accurate for stars later than A0 where the H_2 photo-dissociation timescale is much longer than the system life-time.

^bThe disk is optically thin in these lines for our assumed parameters. Moreover, we assume that all species are in LTE. If the number densities of colliding particles fall below the critical density for LTE, the lines fluxes will be greatly reduced.

our model.

Apart from HR 4796A, there is also a stringent upper-limit on $\text{N}[\text{H}_2]$ in the β Pic disk Lecavelier des Etangs et al. (2001): $\text{N}[\text{H}_2] < 10^{18} \text{cm}^{-2}$. This disk is edge-on, so there is not the same complications in interpreting the column densities as for HR 4796A. Most likely there is not a significant amount of gas in the β Pic disk (also see Fernandez et al. 2006). In corroboration with this conclusion, the disk does not exhibit a narrow dust ring.

• OI 63.2 μm Flux

In the transitional disks we study, the gas is heated by photoelectrons from the dust grains, and cooled mostly by radiation in the OI 63.2 μm line. The estimated line fluxes at the Earth are listed in Table 2.

All objects should be easily detectable by the PACS instrument in the upcoming Herschel mission. For instance, PACS should be able to achieve a $5 - \sigma$ detection of the HR 4796A system in a mere 6 minutes. With a diffraction limit of $\sim 8''$, Herschel may even spatially resolve some of the close-by systems. Metallic gas (C, O, Fe, Na...) has been detected in the β Pic disk (Brandeker et al. 2004;

Roberge et al. 2006). This gas may be produced during collisions of dust grains and contains little or no hydrogen (Fernandez et al. 2006). We calculate the OI/CII fluxes expected in such a hydrogen-poor disk and find them to be comparable to those listed in Table 2. This is because the electron density is not significantly reduced when hydrogen is absent from the gas (§4.1). The photoelectric heating rate remains largely unchanged from that of a hydrogen-rich disk. So even though the total gas mass of the disk is very low, there is good reasons to expect, and therefore to search for, emission in fine-structure cooling lines.

• CII 157.7 μm Flux

Detection of the 157.7 μm CII line has been reported for the β Pic disk (using ISO, Kamp et al. 2003) with a flux of $1.8 \times 10^{-13} \text{erg}/\text{cm}^2/\text{s}$ ($4 - \sigma$ detection). This is ~ 30 times greater than our computed value of $6.0 \times 10^{-15} \text{erg}/\text{cm}^2/\text{s}$ (Table 2) and is surprising.

Ionized carbon has been observed in absorption with a column density of $\text{N}[\text{CII}] \approx 2.5 \times 10^{16} \text{cm}^{-2}$ (Roberge et al. 2006). Without knowing the actual gas/dust masses and distributions, We can obtain an upper limit to the CII flux by assuming that

every CII observed in absorption resides in the excited state and spontaneously radiates. Assuming a vertical scale height of 0.05 and no self-absorption, we obtain a flux of 2.4×10^{-14} erg/cm²/s — still a factor of 10 below that reported by Kamp et al. (2003). More investigation is warranted to resolve this discrepancy.

Looking towards the future, the HIFI instrument on Herschel, with a high frequency cut-off at 1,910 GHz ($\sim 157.0 \mu\text{m}$) and a superb spectral resolution of 5×10^6 , may be capable of detecting this line in debris disks and provide us with detailed kinematics of the gas in these disks.

Within the temperature range relevant to this work, the critical electron number density required for LTE in the OI line is $\sim 10^5/\text{cm}^3$, while it is $\sim 10/\text{cm}^3$ in the CII line. If the disk density falls below these values, the expected line fluxes are greatly reduced from our estimates and the gas temperature rises. Similar values pertain for collisions with hydrogens.

7. COMPLICATIONS

In this section we discuss some complications ignored in our analysis and their impact on our conclusions. This include the roles of grain eccentricities, grain-grain collisions and gas dynamics.

7.1. Eccentric Orbits of Small Grains

Throughout our analysis, we have assumed that grains are on circular orbits. We examine this assumption here.

If grains are produced from larger bodies that are on circular orbits, they would acquire an eccentricity at birth,

$$e = e_{\text{birth}} = \frac{\beta}{1 - \beta} = \frac{s_{\text{min}}}{2s - s_{\text{min}}}, \quad (23)$$

where numerically, $e \sim (s/s_{\text{min}})^{-5/3}$ for $s \sim s_{\text{min}}$. Grains are then launched to highly eccentric orbits with their apastron sorted by their sizes; the dust ring consequently spreads out in the dynamical timescale. Assuming a grain size distribution of $dN_s/ds \propto s^{-\alpha}$, where N_s is defined in eq. [16], and that grains reside only at their apastron, $r \approx r_{\text{ap}} = 70 \times (1+e)/(1-e)$ AU $\sim 140/(1-e)$ AU (for $e \sim 1$), we obtain the following surface brightness profile (eq. [14]):

$$I(r) \propto \frac{s^{2-\alpha}}{r^3} \frac{ds}{de} \frac{de}{dr} \propto \frac{1}{r^5} \left(1 - \frac{140}{r}\right)^{-14/5+3\alpha/5} \propto \frac{1}{r^5}. \quad (24)$$

This profile is insensitive to the value of α (see Fig. 6). Without gas drag this broad surface brightness profile does not evolve with time and conflicts with the appearance of a narrow ring (also see Strubbe & Chiang 2006).

The presence of gas changes this scenario: grain eccentricities are typically damped by collisions with gas particles (which are assumed to be on circular orbits). A grain moving at a velocity $\Delta\mathbf{v}$ relative to the gas feels a drag force (Kwok 1975)

$$\mathbf{F}_{\text{drag}} = -\pi s^2 \rho_{\text{gas}} (v_{\text{th}}^2 + \Delta v^2)^{1/2} \Delta\mathbf{v}, \quad (25)$$

where $v_{\text{th}} = 4/3 \sqrt{8k_B T_{\text{gas}}/\pi \mu m_H}$ is the local thermal speed. The relative velocity (as well as the eccentricity)

can be damped in $\sim T_s$ orbits, where T_s is the dimensionless stopping time (also called the Stokes number):

$$T_s = t_s \Omega_{\text{kep}} = \frac{4\rho_{\text{grain}} s v_{\text{kep}}}{3\rho_g r v_{\text{th}}} \frac{1}{\sqrt{1 + \Delta v^2/v_{\text{th}}^2}}. \quad (26)$$

Here Ω_{kep} is the local Keplerian frequency and $t_s = m_{\text{grain}} \Delta v / F_{\text{drag}}$ is the dimensional stopping time, with $m_{\text{grain}} = 4\pi/3 \rho_{\text{grain}} s^3$. In our fiducial disk, the gas density is so low that all grains are weakly coupled to the gas: T_s ranges from 4 for the smallest grains to 600 for 1 mm grains. Even so, the dimensional stopping time is still short compared to the collision time. So large grains can be assumed to be placed on circular orbits after they are produced. Very small grains (near blow-out size, $s \geq s_{\text{min}}$), however, behave differently.

The highly eccentric orbits ($e_{\text{birth}} \sim 1$) of these very small grains keep them away from the denser inner gas disk for most of their orbits. As a result, the effective stopping time is longer. Moreover, these grains encounter a tail wind near their apastron. For very small grains, this positive torque can exceed the negative torque that they may receive at periastron. They are then migrated outward in addition to being gradually circularized. If the gas disk has an outer edge, the eccentricities of these grains may actually increase (TA01). So it is unreasonable to assume these small grains follow circular orbits with semi-major axes near 70 AU (the production site).

For the temperature profile in Fig. 3, the large-small grain boundary is at $\sim 3.1s_{\text{min}}$, while for that in Fig. 4, the boundary is at $\sim 2.4s_{\text{min}}$. In other words, as the gas temperature rises due to the increasing dust concentration, smaller and smaller grains will be retained within the ring (an instability).

In Fig. 6, we show the surface brightness profile of the dust ring with and without gas drag. Particles of various sizes are produced at 70 AU with the local Keplerian speed. Their dynamics then evolve under the combined forces of gravity, radiation pressure and gas drag (where applicable). In the presence of gas, the dust profile progressively evolves into a sharply defined ring. Note that the local pressure maximum produced by dust heating is essential for containing grains — if the gas has zero pressure gradient or if the gas temperature equals the local dust temperature, all grains are gradually pushed outward.

Lastly, circularization of bigger grains also reduces the birth eccentricity of the small grains — for instance, since the $20 \mu\text{m}$ grains are circularized by gas before they collide to produce the $10 \mu\text{m}$ grains (see Fig. 7), the birth eccentricity for the latter group is reduced from the value in eq. [23] to

$$e_{\text{birth}} \sim \frac{\beta/2}{1 - \beta/2}. \quad (27)$$

This moves the aforementioned large-small boundary to an even smaller value.

These positive feedback effects may in the end lead to trapping of even the smallest grains — an impossible feat when no gas is present. A more complete analysis than that performed here is required, but the presence of non-circular orbits does not seem to change our basic conclusions about narrow-ring formation.

7.2. Grain Collisions

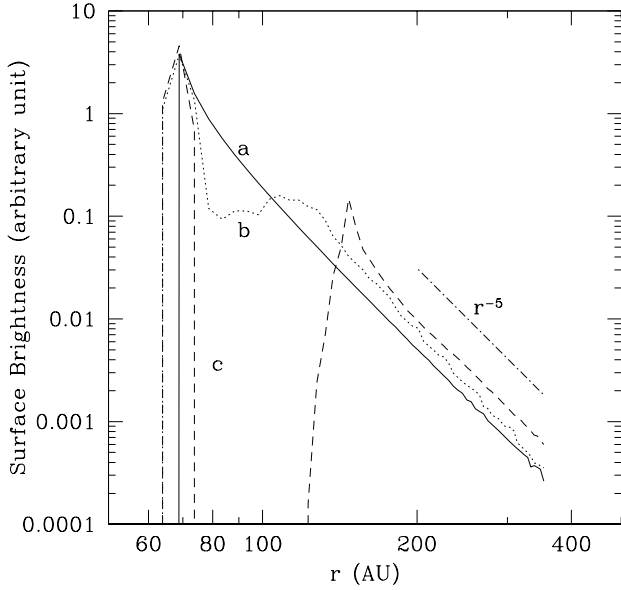


FIG. 6.— Evolution of the surface brightness of a face-on dust disk due to gas drag. Here, dust particles of different sizes (s^{-4} number distribution) are initially produced at 70 AU with the local Keplerian velocity. The surface brightness is plotted (in arbitrary unit) as a function of radius (in AU): (a) when no gas is present (or at time 0); (b) after undergoing gas drag for 10^4 yrs; (c) for 10^5 yrs. Case (c) will be observed as a narrow ring with well-defined edges, confirming the results obtained assuming circular orbits (Fig. 3). The adopted gas parameters are from our fiducial model (temperature as shown in Fig. 3). The dot-dashed line indicates a r^{-5} power law, confirming the result in eq. [24] for the gas-free case.

We have so far ignored the role of grain regeneration by collisions. The importance of collisions can be best studied by comparing different timescales. In Fig. 7, we plot: the orbital period at 70 AU; the timescale for grain collision ($T_{\text{collision}}$) in the initial 20 AU FWHM dust belt; the timescale for a grain to reach its stable orbit ($T_{\text{migration}}$); the timescale for the grains to vertically settle due to gas drag (T_{settle}); the timescale for the grain’s birth eccentricity to be halved by gas drag (T_{circ}); and the timescale for the periastron of small grains to be expanded outwards of 100 AU (T_{expand}). The latter two are relevant for eccentric grains. We adopt the fiducial model (Fig. 3) when calculating these values.

Numerically, we quantify $T_{\text{migration}}$ as the time it takes for a grain originally located at 70 AU to travel a distance of 10 AU (FWHM/2). The radial migration velocity is calculated as follows. In the weak coupling limit, the tangential movement of a grain is not significantly modified by the gas drag, $v_{\theta} = v_{\text{kep}}(1-\beta)^{1/2}$. The gas drag associated with the gas-grain relative velocity removes (injects) angular momentum from (into) the dust grain if the gas moves slower (faster) than the dust, causing a grain of size s to migrate to a radius r where $\beta(s) = \eta(r)$.⁷ The

⁷ The Poynting-Robertson drag is insignificant in comparison to the gas drag.

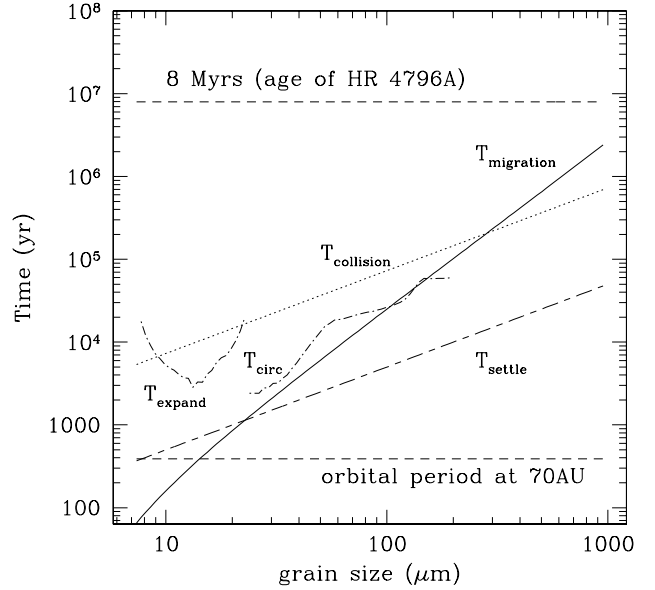


FIG. 7.— Various timescales in our fiducial model are plotted here as functions of grain size. $T_{\text{migration}}$ is the radial migration timescale for grains to move by half the original FWHM of the dust belt. $T_{\text{collision}}$ is the collision timescale between grains of comparable sizes in the belt. T_{settle} is the vertical settling time for a grain due to gas drag. The two dot-dashed curves represent T_{circ} and T_{expand} , which are relevant for eccentric grains (§7.1): the former is the timescale for gas drag to damp the grain birth eccentricity, while the latter is the timescale for the periastron of small grains to be pushed outwards of, say, 100 AU, by which distance they can no longer affect the narrow ring appearance. The dashed lines denote the estimated age for the HR 4796A system and the orbital period at 70 AU, respectively. The Poynting-Robertson drag timescale is comparable to the system lifetime even for $10 \mu\text{m}$ grains, and is much longer for larger grains. We set $\eta = 0$ for simplicity when calculating $T_{\text{migration}}$.

grains migrate radially with a velocity (cf. TA01 eq. [23])

$$v_{\text{rad}} = \frac{2}{T_s} \left[\left(\frac{1-\eta}{1-\beta} \right)^{\frac{1}{2}} - 1 \right] v_{\text{kep}}. \quad (28)$$

Circular grains ($s \geq 300 \mu\text{m}$) typically encounter multiple collisions – and possibly grind down to smaller grains – before they reach their respective stable orbits. This allows small grains to be regenerated continuously even if they are initially lost from the system due to gas drag. Grains smaller than $\sim 300 \mu\text{m}$ can migrate to their stable orbits before colliding destructively with grains of a similar size.

When grain eccentricities are considered (eq. [23]), all grains greater than $\sim 20 \mu\text{m}$ will be trapped in the ring and are circularized faster than their collision lifetime – their collisional progeny will likely obtain a birth eccentricity closer to that in eq. [27] than that in eq. [23], and are therefore easier to trap in the ring. Grains of size $\sim 10 - 20 \mu\text{m}$ ⁸ are depleted from the ring faster than they can collisionally break-down ($T_{\text{expand}} \ll T_{\text{collision}}$)

⁸ When the gas temperature is raised further due to the enhanced dust concentration, these sizes are reduced to smaller values.

– or more relevantly, they are removed faster than they can be regenerated from larger grains. So these grains will not destroy the narrow ring appearance. Very small grains ($7 - 8 \mu\text{m}$) are removed more slowly. However, their very large apastron also means that they do not matter much for the narrow ring appearance.

In summary, grain collisions do not seem to adversely affect our theory.

7.3. Gas Dynamics

We have ignored all dynamical responses of the gas to the heating and the migration of the dust. The gas may expand vertically due to the heating, and expand radially as the dust is concentrated. Moreover, such an optically thin disk most likely experiences a macroscopic viscosity due to MHD turbulence. How does gas dynamics impact the ring instability?

In §6 we argue that there is little vertical expansion of the gas within the heated regions of the disk. Because the gas is heated or cooled faster than the vertical sound crossing time, gas temperature at every altitude is determined by the local heating and cooling. Gas high above the mid-plane is heated to a temperature lower than that at the mid-plane, since the photoelectric heating yield there is lower.⁹ The overall vertical scale height is thus determined, not by the mid-plane temperature, but by that of the dust disk. This justifies our fiducial choice of setting H/r of the gas and dust components to be equal.

As dust is concentrated into a narrow ring, the gas is expelled away from the ring by action-reaction, which lowers the local gas density and reduces the pressure gradient. This negative feedback only occurs because grains are being concentrated. It is a higher order effect that acts to limit the amplitude, but not change the sign, of the instability.

Viscosity tends to erase the (angular) velocity gradient and dissipate the gas disk. However, if the ring is ~ 10 AU in width, the viscous time across the ring is ~ 0.5 Myr (taking a Shakura-Sunyaev $\alpha = 10^{-2}$, $H/r = 0.05$). As a result, the velocity gradient can be actively maintained by dust heating. Gas dissipation occurs over a few Myr timescale and may eventually terminate the ring instability.

8. CONCLUSIONS

We have studied the thermal and dynamical consequences of an optically thin dust disk embedded in a gas

⁹ This conclusion can reverse when one considers NLTE cooling.

disk of comparable mass. We showed that photoelectric emission from the dust grains heats up the gas and this modifies the grains' orbital motion: if the dust is produced in a belt-like region (like that of our Kuiper belt), the heated gas will collect dust particles into a narrower region with sharp edges. This resulting dust distribution may be associated with the dust rings observed in various debris disks, such as that around HR 4796A, and possibly HD 105.

This mechanism operates around stars with a spectral type at late as K2 and is valid for gas and dust masses over ~ 2 orders of magnitude in range. So, if every circumstellar disk goes through a transitional stage as we have described here, a narrow dust ring is expected to form. However, it is likely that the ring will disperse as the gas dissipates.

We have restricted ourselves to consider only axisymmetric rings; an interesting extension of this work will be to explore whether non-axisymmetric features may also derive from gas-dust interaction. We have also considered the impact of eccentricities induced by radiation pressure on small grains that are released from larger bodies on circular orbits. This process complicates our theory, but does not diminish the instability.

We conclude that the presence of narrow dust rings in optically thin, transitional-stage disks, such as that observed around HR 4796A, does not necessarily imply the presence of “shepherding” planets. Instead, we argue that the detection of narrow dust rings may indicate the presence of gas. We have shown that this conclusion is compatible with the stringent upper limit on the H_2 column density in the HR 4796A disk.

Lastly, most of the gas cooling occurs via the OI or CII infrared lines. We have computed the expected fluxes for various systems and point out that the upcoming Herschel mission will be instrumental in observing and characterizing the gas.

We thank an anonymous referee for careful readings and many constructive comments. Thanks are also due to Alexis Brandeker, Ray Jayawardhana, Rodrigo Fernandez and Kyryl Zagarovky for help and discussions. This research was supported by the National Science and Engineering Research Council of Canada, through a discovery grant to YW and an NSERC undergraduate student research award to GB.

REFERENCES

- Alexander, R. D., Clarke, C. J., & Pringle, J. E. 2006, MNRAS, 369, 229
- Ardila, D. R., Golimowski, D. A., Krist, J. E., Clampin, M., Williams, J. P., Blakeslee, J. P., Ford, H. C., Hartig, G. F., & Illingworth, G. D. 2004, ApJ, 617, L147
- Augereau, J. C., Nelson, R. P., Lagrange, A. M., Papaloizou, J. C. B., & Mouillet, D. 2001, A&A, 370, 447
- Aumann, H. H. 1985, PASP, 97, 885
- Aumann, H. H., Beichman, C. A., Gillett, F. C., de Jong, T., Houck, J. R., Low, F. J., Neugebauer, G., Walker, R. G., & Wesselius, P. R. 1984, ApJ, 278, L23
- Backman, D. & Paresce, F. 1993, in Protostars and Planets, ed. E. Levy & J. Lunine, Vol. III (Univ. Arizona Press), 1253
- Barrado y Navascues, D., Stauffer, J. R., Hartmann, L., & Balachandran, S. C. 1997, ApJ, 475, 313
- Brandeker, A., Liseau, R., Olofsson, G., & Fridlund, M. 2004, A&A, 413, 681
- Chen, C. H. & Kamp, I. 2004, ApJ, 602, 985
- Currie, T., Semenov, D., Henning, T., Furlan, E., & Herter, T. 2003, in ASP Conf. Ser. 294: Scientific Frontiers in Research on Extrasolar Planets, 265
- Dent, W. R. F., Greaves, J. S., & Coulson, I. M. 2005, MNRAS, 359, 663
- Dent, W. R. F., Walker, H. J., Holland, W. S., & Greaves, J. S. 2000, MNRAS, 314, 702

- Di Folco, E., Thévenin, F., Kervella, P., Domiciano de Souza, A., Coudé du Foresto, V., Ségransan, D., & Morel, P. 2004, *A&A*, 426, 601
- Dohnanyi, J. W. 1969, *J. Geophys. Res.*, 74, 2531
- Draine, B. T. 1978, *ApJS*, 36, 595
- Fernandez, R., Brandeker, A., & Wu, Y. 2006, *ApJ*, 643, 509
- Fixsen, D. J. & Dwek, E. 2002, *ApJ*, 578, 1009
- Gorti, U. & Hollenbach, D. 2004, *ApJ*, 613, 424
- Greaves, J. S., Holland, W. S., Wyatt, M. C., Dent, W. R. F., Robson, E. I., Coulson, I. M., Jenness, T., Moriarty-Schieven, G. H., Davis, G. R., Butner, H. M., Gear, W. K., Dominik, C., & Walker, H. J. 2005, *ApJ*, 619, L187
- Greaves, J. S., Mannings, V., & Holland, W. S. 2000, *Icarus*, 143, 155
- Goldreich, P., Lithwick, Y., & Sari, R. 2004, *ARA&A*, 42, 549
- Habing, H. J. 1968, *Bull. Astron. Inst. Netherlands*, 19, 421
- Hauschildt, P. H., Allard, F., & Baron, E. 1999, *ApJ*, 512, 377
- Heap, S. R., Lindler, D. J., Lanz, T. M., Cornett, R. H., Hubeny, I., Maran, S. P., & Woodgate, B. 2000, *ApJ*, 539, 435
- Holland, W. S., Greaves, J. S., Dent, W. R. F., Wyatt, M. C., Zuckerman, B., Webb, R. A., McCarthy, C., Coulson, I. M., Robson, E. I., & Gear, W. K. 2003, *ApJ*, 582, 1141
- Hollenbach, D., Gorti, U., Meyer, M., Kim, J. S., Morris, P., Najita, J., Pascucci, I., Carpenter, J., Rodmann, J., Brooke, T., Hillenbrand, L., Mamajek, E., Padgett, D., Soderblom, D., Wolf, S., & Lunine, J. 2005, *ApJ*, 631, 1180
- Hollenbach, D. & McKee, C. F. 1979, *ApJS*, 41, 555
- Jayawardhana, R., Fisher, S., Hartmann, L., Telesco, C., Pina, R., & Fazio, G. 1998, *ApJ*, 503, L79
- Jonkheid, B., Faas, F. G. A., van Zadelhoff, G.-J., & van Dishoeck, E. F. 2004, *A&A*, 428, 511
- Jura, M. 2004, in *ASP Conf. Ser. 324: Debris Disks and the Formation of Planets*, ed. L. Caroff, L. J. Moon, D. Backman, & E. Praton, 93
- Jura, M., Malkan, M., White, R., Telesco, C., Pina, R., & Fisher, R. S. 1998, *ApJ*, 505, 897
- Kalas, P., Graham, J. R., & Clampin, M. 2006, *ApJ*, 637, L57
- , 2005, *Nature*, 435, 1067
- Kamp, I. & Bertoldi, F. 2000, *A&A*, 353, 276
- Kamp, I. & Dullemond, C. P. 2004a, *ApJ*, 615, 991
- , 2004b, *ApJ*, 615, 991
- Kamp, I. & van Zadelhoff, G.-J. 2001, *A&A*, 373, 641
- Kamp, I., van Zadelhoff, G.-J., van Dishoeck, E. F., & Stark, R. 2003, *A&A*, 397, 1129
- Kenyon, S. J. & Bromley, B. C. 2004a, *AJ*, 127, 513
- , 2004b, *ApJ*, 602, L133
- , 2002, *ApJ*, 577, L35
- , 2001, *ApJ*, 121, 538
- Kenyon, S. J., Wood, K., Whitney, B. A., & Wolff, M. J. 1999, *ApJ*, 524, L119
- Klahr, H. & Lin, D. 2005, *ApJ*, 632, 1113
- Koerner, D. W., Ressler, M. E., Werner, M. W., & Backman, D. E. 1998, *ApJ*, 503, L83
- Krauss, O. & Wurm, G. 2005, *ApJ*, 630, 1088
- Krivov, A. V., Lohne, & T., Sremcevic, M. 2006, *â455*, 509, (DOI: 10.1051/0004-6361:20064907)
- Kuchner, M. J. & Holman, M. J. 2003, *ApJ*, 588, 1110
- Kwok, S. 1975, *ApJ*, 198, 583
- Lecavelier des Etangs, A., Vidal-Madjar, A., Roberge, A., Feldman, P. D., Deleuil, M., André, M., Blair, W. P., Bouret, J.-C., Désert, J.-M., Ferlet, R., Friedman, S., Hébrard, G., Lemoine, M., & Moos, H. W. 2001, *Nature*, 412, 706
- Mannings, V. & Barlow, M. J. 1998, *ApJ*, 497, 330
- Marsh, K. A., Velusamy, T., Dowell, C. D., Grogan, K., & Beichman, C. A. 2005, *ApJ*, 620, L47
- Mayer, M. & Duschl, W. J. 2005, *MNRAS*, 358, 614
- Meyer, M. R., Backman, D. E., Weinberger, A. J., & Wyatt, M. C. 2006, in *Protostars and Planets V*, Chapters 6, University of Arizona Press
- Meyer, M. R., Hillenbrand, L. A., Backman, D. E., Beckwith, S. V. W., Bouwman, J., Brooke, T. Y., Carpenter, J. M., Cohen, M., Gorti, U., Henning, T., Hines, D. C., Hollenbach, D., Kim, J. S., Lunine, J., Malhotra, R., Mamajek, E. E., Metchev, S., Moro-Martín, A., Morris, P., Najita, J., Padgett, D. L., Rodmann, J., Silverstone, M. D., Soderblom, D. R., Stauffer, J. R., Stobie, E. B., Strom, S. E., Watson, D. M., Weidenschilling, S. J., Wolf, S., Young, E., Engelbracht, C. W., Gordon, K. D., Misselt, K., Morrison, J., Muzerolle, J., & Su, K. 2004, *ApJS*, 154, 422
- Moran, S. M., Kuchner, M. J., & Holman, M. J. 2004, *ApJ*, 612, 1163
- Moro-Martín, A., Wolf, S., & Malhotra, R. 2005, *ApJ*, 621, 1079
- Nagasawa, M., Thommes, E. W., Kenyon, S. J., Bromley, B. C., & Lin, D.N.C., 2006, in *Protostars and Planets V*, Chapter 7, University of Arizona Press
- Olofsson, G., Liseau, R., & Brandeker, A. 2001, *ApJ*, 563, L77
- Osterbrock, D. E. & Ferland, G. J. 2006, *Astrophysics of gaseous nebulae and active galactic nuclei* (Astrophysics of gaseous nebulae and active galactic nuclei, 2nd. ed. by D.E. Osterbrock and G.J. Ferland. Sausalito, CA: University Science Books, 2006)
- Ozernoy, L. M., Gorkavyi, N. N., Mather, J. C., & Taidakova, T. A. 2000, *ApJ*, 537, L147
- Quillen, A. C. & Thorndike, S. 2002, *ApJ*, 578, L149
- Roberge, A., Feldman, P. D., Lagrange, A. M., Vidal-Madjar, A., Ferlet, R., Jolly, A., Lemaire, J. L., & Rostas, F. 2000, *ApJ*, 538, 904
- Roberge, A., Feldman, P. D., Weinberger, A. J., Deleuil, M., & Bouret, J.-C. 2006, *Nature*, 441, 724
- Roberge, A., Weinberger, A. J., Redfield, S., & Feldman, P. D. 2005, *ApJ*, 626, L105
- Schneider, G., Silverstone, M. D., Hines, D. C., Augereau, J.-C., Pinte, C., Menard, F., Krist, J., Clampin, M., Grady, C., Golimowski, D., Ardila, D., Henning, T., Wolf, S. & Rodman, J. 2006, *astro-ph/0606213*
- Schneider, G., Smith, B. A., Becklin, E. E., Koerner, D. W., Meier, R., Hines, D. C., Lowrance, P. J., Terrile, R. J., Thompson, R. I., & Rieke, M. 1999, *ApJ*, 513, L127
- Song, I., Caillault, J.-P., Barrado y Navascués, D., Stauffer, J. R., & Randich, S. 2000, *ApJ*, 533, L41
- Spitzer, L. J. & Tomasko, M. G. 1968, *ApJ*, 152, 971
- Stauffer, J. R., Hartmann, L. W., & Barrado y Navascués, D. 1995, *ApJ*, 454, 910
- Stewart, G. R. & Wetherill, G. W. 1988, *Icarus*, 74, 542
- Strom, S. E. & Edwards, S. 1993, in *ASP Conf. Ser. 36: Planets Around Pulsars*, 235
- Strubbe, L. E. & Chiang, E. I. 2006, *ApJ*, 648, 652
- Su, K., Rieke, G. H., Misselt, K. A., Stansberry, J. A., Moro-Martín, A., Stapelfeldt, K. R., Werner, M. W., Trilling, D. E., Bendo, G. J., Hines, D. C., Wyatt, M. C., Holland, W. S., Marengo, M., Megeath, S. T., & Fazio, G. G. 2005, *ApJ*, 628, 487
- Takeuchi, T. & Artymowicz, P. 2001, *ApJ*, 557, 990
- Thébaud, P., Augereau, J. C., & Beust, H. 2003, *A&A*, 408, 775
- Weingartner, J. C. & Draine, B. T. 2001, *ApJS*, 134, 263
- Williams, J. P., Najita, J., Liu, M. C., Bottinelli, S., Carpenter, J. M., Hillenbrand, L. A., Meyer, M. R., & Soderblom, D. R. 2004, *ApJ*, 604, 414
- Wilner, D. J., Holman, M. J., Kuchner, M. J., & Ho, P. T. P. 2002, *ApJ*, 569, L115
- Wyatt, M. C. 2006, *ApJ*, 639, 1153
- , 2005, *A&A*, 433, 1007
- , 2003, *ApJ*, 598, 1321
- Zuckerman, B. & Becklin, E. E. 1993, *ApJ*, 414, 793
- Zuckerman, B., Song, I., Bessell, M. S., & Webb, R. A. 2001, *ApJ*, 562, L87